Journal of Computational and Applied Mechanics, Vol. 8., No. 2., (2007), pp. 211–223

3D UNSTEADY FLOW IN A CENTRIFUGAL FAN: IMPELLER - VOLUTE INTERACTION

Mohand Younsi, Farid Bakir, Smaine Kouidri and Robert Rey
Laboratoire d'Energétique et de Mécanique des Fluides Interne LEMFI - ENSAM
151 Boulevard de l'Hôpital 75013 Paris, France
mohand.younsi@paris.ensam.fr

[Received: January 15, 2007]

Abstract. The purpose of this study is to show, using Computational Fluid Dynamics (CFD) tools, the complex phenomena related to the internal flow in a squirrel-cage fan and their influence on the aeroacoustic behaviour. These phenomena are the interactions and unsteadiness induced by the relative motion of the rotating blades compared to the volute. Thus, 3D unsteady calculation using the Unsteady Reynolds Averaged Navier-Stokes (URANS) approach has been applied on the computational domains which have been divided into two zones, a rotating zone including the impeller and a stationary zone including the volute. The sliding mesh technique has been applied to the interfaces in order to allow the unsteady interactions between the two zones. The overall behaviour of the fan has been validated experimentally at different flow rates. The unsteady part is illustrated by the pressure and aerodynamic force fluctuations applied on the blade surfaces, and on different points from the lateral surface of the volute. Finally, using the pressure and the velocity fluctuations data acquired upon the surfaces of rotating blades, acoustic pressures have been computed using the Fowcs Williams-Hawking (FW-H) analogy.

Keywords: aeroacoustics, centrifugal fan, CFD, turbomachinery

Nomenclature

a_0	$[m/s]$	Sound speed in quiescent medium
$f=0$	$[-]$	Function describing the source surface
F	$[Hz]$	Frequency
G	$[-]$	$=\tau - t + r/c$
$H(f)$	$[-]$	Heaviside function
M	$[-]$	Local Mach number vector of source with respect to a frame fixed to the undisturbed medium, with components M_i
n_j	$[-]$	Unit normal vector
p'	$[Pa]$	Acoustic pressure
P_{ij}	$[Pa]$	Compressive stress tensor
p_{ref}	$[Pa]$	Reference pressure
Psd	$[Pa^2]$	Power spectral density
R	$[m]$	Distance between observer and source

t	$[s]$	Observer time
T_{ij}	$[Pa]$	Lightill stress tensor
u_i	$[m/s]$	Fluid velocity in the xi direction
u_n	$[m/s]$	Fluid velocity in the normal direction
v_i	$[m/s]$	Surface velocity in the x_i direction
v_n	$[m/s]$	Surface velocity in the normal direction
x	$[m]$	Observer position
$\delta(f)$	$[-]$	Dirac delta function
Δt	$[s]$	Time step
ρ	$[kg/m^3]$	Density
τ	$[s]$	Source time

Subscripts

L	Loading noise component
T	Thickness noise component
0	Fluid variable in quiescent medium

1. **Introduction**

Squirrel-cage centrifugal fans are widely used in industry. They are used as circulating fans in central heating and air-conditioning systems in buildings, as blowers in automotive heating/cooling units, and in numerous other applications for their high capacity of mass flow, size compactness and low noise.

Many authors have worked in the study of unsteady phenomena in turbomachines. These phenomena are the interactions and unsteadiness induced by the motion of the rotor relatively to the stator.

Concerning centrifugal fans, M. Gabi and T. Klemm [1] used a numerical method based on a CFD analysis, and an experimental method using Particle Image Velocimetry (PIV) in order to predict the performance characteristics and flow data of cross-flow fans. Sandra Velarde-Suarez [2] studied the aeroacoustic behaviour based on the theory of vortex sound coupled with experimental data. Siddharth Thakur [3] used three dimensional (3D) CFD approach to analyze fluid flow in a centrifugal fan. Yong Cho and Young J.Moon [4] used the unsteady viscous flow fields of a cross-flow fan computed by solving the two dimensional (2D) incompressible Navier-stokes equations in order to feed the FW-H equation. They studied the acoustic benefit of an impeller with uneven blade spacing. Kwang-Yong Kim [5] applied the response surface method using RANS approach to the aerodynamic design of a forward-curved-blade centrifugal fan to optimize the shapes of scroll and blades in order to maximize flow efficiency.

In this paper, interactions and unsteadiness induced by the motion of rotating blades relatively to the volute have been studied using CFD calculations. The overall behaviour of the fan has been validated experimentally at different flow rates. The unsteady part of this study is illustrated by the pressure and aerodynamic force fluctuations applied on blade surfaces, and on different points from the lateral surface

of the volute. The analysis of the wake generated by the rotation of the blower shows that the volute tongue is the main zone of unsteadiness and flow perturbations.

Finally, based on pressure fluctuations data acquired upon the surfaces of rotating blades, acoustic pressures have been computed at the far field using the FW-H formalism.

2. **Fan presentation**

The main fan parameters are presented in Table 1. These parameters have been transformed into a complete Computer Aided Design (CAD) model and saved into STL format in order to build a prototype using the rapid prototyping method which requires that parts are complete and have continuity.

Table 2. Geometrical characteristics values

Impeller	
Description	Value
Blade number	39
Impeller width	70 mm
Blade chord length	26.2 mm
Blade thickness	1 mm
Inlet blade angle	5°
Outlet blade angle	70°
Shape blade	*circular arc*
Rotational speed	3000 rpm
Impeller inlet diameter	120 mm
Impeller outlet diameter	160 mm
Volute casing	
Description	Value
Inlet diameter	120 mm
Outlet size	100 x 76 mm
Volute tongue radius	5 mm
Volute tongue position	*Radius* 90 mm
Volute shape	*Logarithmic law*

3. **Numerical simulation**

The numerical simulations have been carried out using the commercial code FLUENT 6.2. The flow solver used in this code employs for unsteady turbulent flow the three dimensional time-averaged Navier-Stokes equations.

The geometrical parameters given in Table 1 have been used in order to generate the computational domain which has been divided into two zones, a rotational zone including the impeller and stationary zones elsewhere. This configuration takes into

account the clearance between the impeller and the volute. Therefore, the inlet and outlet surfaces of the fan have been extended in order to ensure numerical stability and to minimize boundary condition effects. The computational domain obtained is shown in Figure 1.

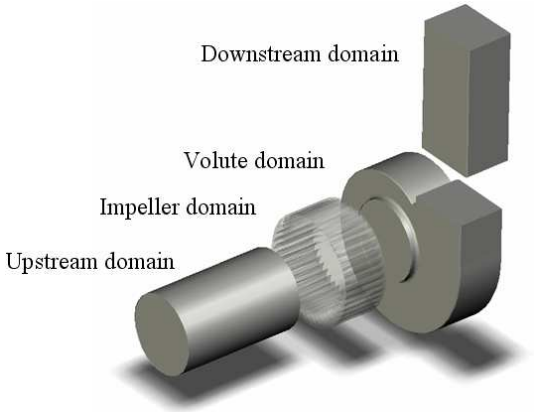

Figure 1. Computational domains

The resulting geometry has been used to build an unstructured grid mesh whose refinement has been studied and adapted to the flow morphology, minimizing element distortion and having the required resolution in high gradient regions. These regions concern essentially the volute tongue zone and the axial gap between the impeller and the volute casing where the flow could present recirculation and perturbations. Using

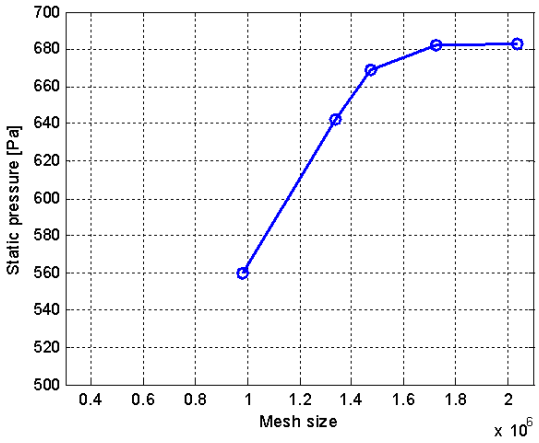

Figure 2. Influence of grid size on the solution

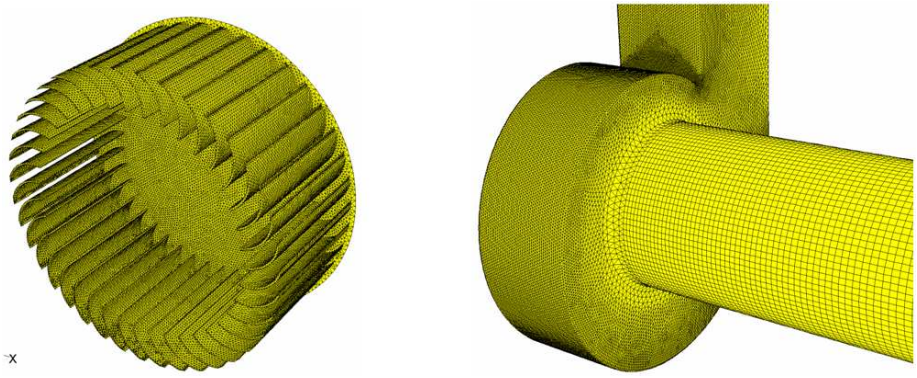

Figure 3. Grids of the computational domain

this generation mesh technique, the difference of static pressure between the inlet and the outlet of the fan has been computed with steady state calculations applied on each generated grid. The result of this analysis is shown in Figure 2. According to this figure, the $1.7x10^6$ cell grid presents a good compromise between mesh independence and Computing Processing Unit (CPU) time. Figure 3 shows the resulting mesh and details of the retained grid are given in Table 2.

Table 3. Retained grid characteristics

Fluid domain	Surface mesh	Solid mesh	Mean size	Number of cells
Impeller	Tri.	hybrid	2 (surf), 3 (solid)	999744
Volute casing	Tri.	hybrid	2 (surf), 5 (solid)	503120
Upstream extent	-	hex	5	60600
Downstream extent	Tri.	hybrid	5	160240
			Total	1723704

Concerning the numerical simulation parameters, the CFD simulation process began with a steady flow calculation with a multiple frame of reference based on the frozen-rotor approach. In this case, the relative position of the impeller and casing does not change during the calculations. For unsteady calculations, the sliding mesh technique has been applied on the interfaces in order to allow the unsteady interactions between the impeller and the volute. For each time step, the grids change their relative position during the calculations according to the angular velocity of the impeller. Velocity Inlet and Pressure Outlet boundary conditions have been applied at the inlet and the outlet, respectively. Turbulence has been modeled with the $k-\omega-Shear\ Stress$ (SST) model. The $k-\omega-Shear\ Stress$ model combines the standard $k-\omega$ model with the Standard $k-\varepsilon$ and also takes the transport effects of the principal turbulent shear stress into account through a modified turbulent viscosity formulation. The stopping criterion for the scaled norm of the residuals is set to 10^{-4}. The governing equations have been solved using the segregated solver and a

centred SIMPLE algorithm has been used for the pressure velocity coupling. A gauge pressure of 101325 *Pascal* has been applied at the outlet and a suitable value has been determined for the inlet.

The time step of the unsteady calculations has been set to 5.10^{-5} seconds; this time step is related to the rotational speed of the impeller and it is small enough to capture the phenomena due to the blades' passage and their interactions with the volute casing wall. It corresponds to 1/400 of blade passing period.

4. **Overall performance validation**

Overall measurements have been carried out on the test bench shown in Figure 4, designed and built at LEMFI-ENSAM according to the ISO 5801 standard [6]. It is composed of an airtight box ($1.3x1.3x1.8\ m$), which is placed upstream the centrifugal fan, making it possible to vary the flow rate by changing the diameter of an orifice plate (diaphragm). The rotational speed is set by a frequency variator and measured using an optical tachometer of 0.1 % accuracy. For each diaphragm of given diameter, the static pressure provided by the centrifugal fan is measured using a micro manometer (precision 1 %).

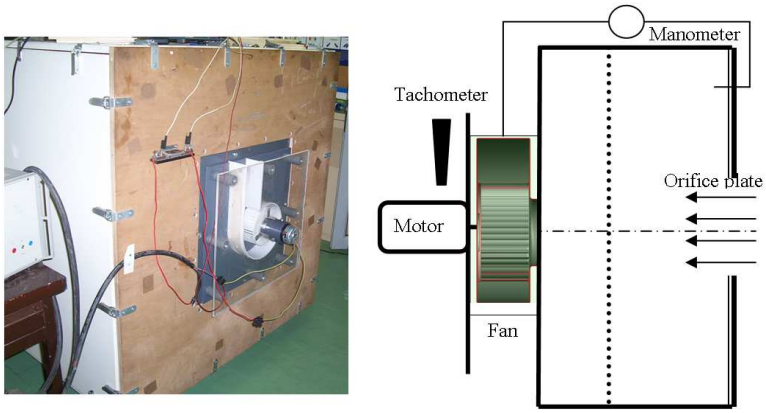

Figure 4. Test bench ISO 5801

Numerical simulations have been carried out at different flow rates. Figure 5 shows the fan static pressure against flow rate and its comparison with the experimental data. It can be seen that the measured static pressure difference between the inlet and the outlet fan is in good agreement with CFD calculations. At partial flow rate, the 3D computation and experimental results does not match; this phenomenon is due to the presence of strong flow recirculation which has not been adequately predicted by the numerical modeling.

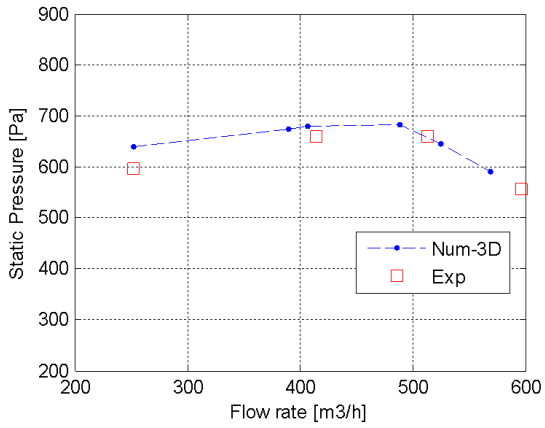

Figure 5. Aerodynamic performance of the centrifugal fan

5. **Pressure and velocity fields**

Figure 6 shows the instantaneous static pressure field at the median surface of the fan at the nominal flow rate (500 m^3/h). The conversion of dynamic pressure produced by the impeller rotation into static pressure by the volute casing can be seen, thus the maximum of pressure is obtained in the outlet duct. A non-homogenous pressure distribution is observed at the zone around the gap between volute tongue and impeller periphery, characterized by a high gradient of pressure. The volute tongue whose role is to drive the flow towards the fan outlet also presents a singularity for the flow. The shape of the volute casing creates a geometrical asymmetry, this phenomenon influences the pressure distribution and fluctuating efforts on the blades impeller. The absolute velocity vectors in the fan are plotted in Figure 7 at the median surface of the fan. The volute tongue zone presents a strong recirculation of the fluid particles in the gap between the volute tongue and the impeller periphery.

In the meridian surface, it can be seen that the impeller blades are partially fed by the flow. This non homogenous distribution of the mass flow coupled with the rectangular shape of the volute casing creates strong vortici and recirculation of the fluid at the axial gap, this phenomenon generates aerodynamic losses.

6. **Unsteady calculations and results**

The different positions around the volute in the middle span (Span 2), where fluctuating static pressure has been calculated (Points 1 to 9) are shown in Figure 6. The same distribution of points has been used in two other parallel spans, Span 1 near the inlet of the fan, and Span 3 in the bottom of the volute. For each time step, the data have been saved. After windowing the temporal signals using Hamming's window function, each recorded sample has been Fast Fourier Transform (FFT) processed (reference pressure is set to $2x10^{-5}$ Pa). The aerodynamic pressure spectra

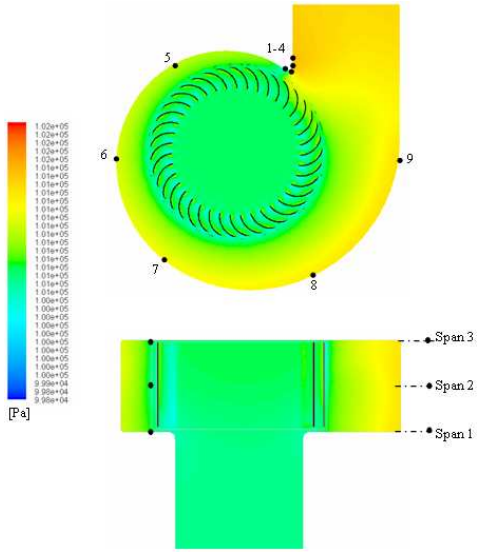

Figure 6. Static pressure field: middle surface and meridian surface of the fan

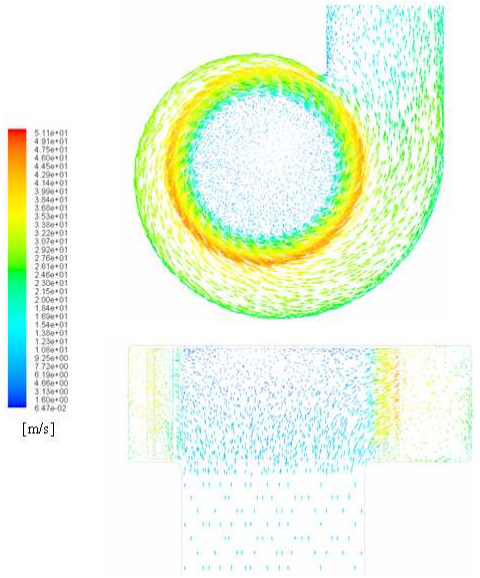

Figure 7. Absolute velocity field: middle surface and meridian surface of the fan

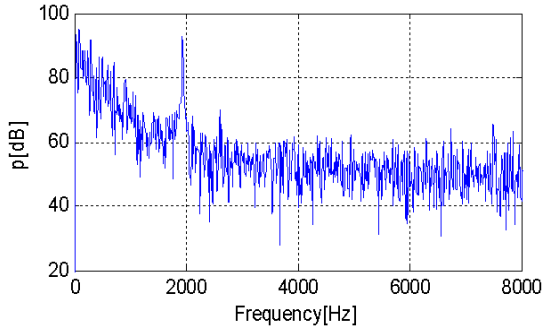

Figure 8. Aerodynamic pressure spectrum at the volute tongue

have been finally obtained. These spectra provide a direct measure of the amplitude of the aerodynamic pressure fluctuations at each frequency.

Figure 8 shows the spectrum of the aerodynamic pressure calculated at the volute tongue in Span 2. The graph suggests that the dominant mode occurs at 1950 Hz, which corresponds to the blade passing frequency (BPF). A non-presence of other peaks in the spectrum at the harmonics frequency is observed. This is due to the nature of the interaction between the impeller and the volute, which does not generate interferences.

The Fourier coefficient values at the BPF point, at each computation point, and at the three defined spans have been calculated and reported in the graph shown in Figure 9. The graph represents the magnitude of the wake generated by the blades motion around the volute. The shapes of the three curves globally match. The dominant value is observed at the volute tongue point; this result indicates that the volute tongue is the main zone of unsteadiness and interaction with the rotating impeller. Away from the volute tongue the three curves decrease, thus the minimum

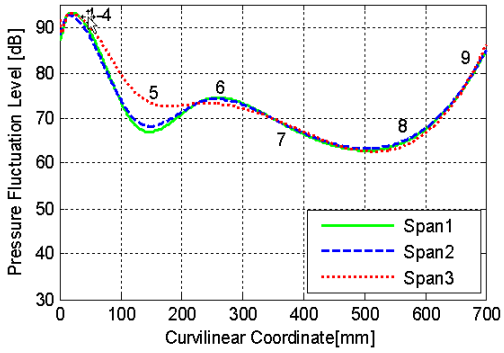

Figure 9. Pressure fluctuation level around the volute at the BPF (1950 Hz)

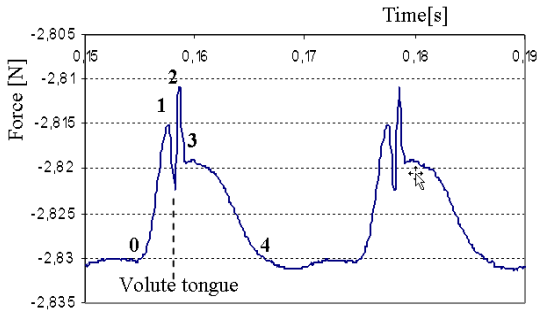

Figure 10. Force fluctuations applied on the blade (2 revolutions)

value is observed in the zone around Point 7, this is due to the morphology of the flow which becomes stable. The curves increase progressively from Point 7 on. It can be seen that Point 6 is remarkable because the curve increases, this is due to the flow which becomes disorganized and it can be related to the volute tongue effect.

Figure 10 shows two periods of the force fluctuations applied on one blade. The total force component on the blade has been computed from the node value by summing the pressure and viscous forces of each cell. According to this diagram, the influence of the volute tongue on the force variation can be seen between Point 1 and Point 3. A quick fluctuation at Point 2 (two milliseconds between Points 1 and 3) is observed. This fast variation has a significant impact on the loading noise generation defined in Section 8.

7. **Aeroacoustic modeling and results**

The FW-H [7] equation is essentially an inhomogeneous wave equation that can be derived manipulating the continuity equation and the Navier-Stokes equations. The FW-H equation can be written as:

$$\begin{aligned} \frac{1}{a_0^2}\frac{\partial^2 p'}{\partial t^2} - \bigtriangledown^2 p' &= \frac{\partial\{[\rho_0 v_n + \rho(u_n - v_n)]\delta(f)\}}{\partial t} - \frac{\partial\{[P_{ij}n_j + \rho u_i(u_n - v_n)]\delta(f)\}}{\partial x_i} + \\ &+ \frac{\partial^2}{\partial x_i \partial x_j}\left[T_{ij}H(f)\right], \end{aligned} \tag{7.1}$$

where:

$$T_{ij} = \rho u_i u_j + P_{ij} - a_0^2(\rho - \rho_0)\delta_{ij} \tag{7.2}$$

$$P_{ij} = p\delta_{ij} - \mu\left[\frac{\partial u_i}{\partial x_j} + \frac{\partial u_j}{\partial x_i} + \frac{2\partial u_k}{3\partial x_k}\delta_{ij}\right] \tag{7.3}$$

The first two source terms in equation (7.1) are monopole (thickness) and dipole (loading) sources, respectively, based on their mathematical structures. The monopole source term models the noise generated by the displacement of fluid as the body passes. The dipole or loading source term models the noise that results from the

unsteady motion of the force distribution on the body surface. Both of these sources are surface sources: i.e. they act only on the surface $f = 0$ as indicated by the Dirac delta function $\delta(f)$. The third source term is a quadrupole source term that acts throughout the volume that is exterior to the data surface as indicated by the Heaviside $H(f)$.

Using the free-space Green function $(\delta(G)/4\pi r)$, the solution to equation (7.1) is obtained. Thus the complete solution consists of surface integrals and volume integrals. The surface integrals represent the contribution from monopole and dipole acoustic sources and partially from quadrupole sources if the integration surface is impermeable. The contribution of the volume integrals which represent quadrupole (volume) sources in the region outside the source surface becomes small when the flow is subsonic. Thus the volume integrals are neglected.

Finally:

$$p'(\mathbf{x},t) = p'_T(\mathbf{x},t) + p'_L(\mathbf{x},t) \ . \tag{7.4}$$

The two terms on the right in equation (7.4), and, thickness and loading terms, respectively, are developed in [8].

The fluctuating variables, pressure and velocity upon the impeller surfaces, have been obtained for 2000 time steps. Then, sound pressure signals have been computed at the receiver location using the source data collected during the aerodynamic calculation. For the time step selected here $(5x10^{-5}s)$, the highest frequency that the acoustic analysis can produce is:

$$F = \frac{1}{2\Delta t} 10 \ kHz.$$

Figure 11 shows the sound pressure level spectrum of the impeller computed one meter away from the axis of the fan at the exit duct. This position is selected in order to compute the sound pressure level according to the free field radiation condition.

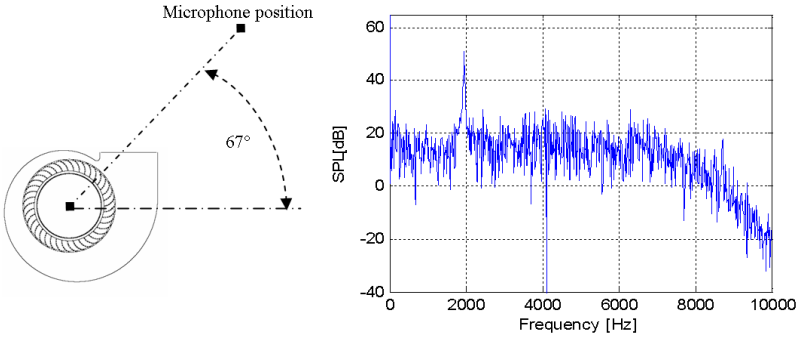

Figure 11. Microphone position and corresponding spectrum radiated by the impeller

It can be seen that there is one dominant peak: this peak occurs at 1950 Hz, which corresponds to the blade passing frequency. Amplitude of 51 dB at this frequency is noticed. The non-presence of other harmonics is due to the geometrical shape of the volute casing interacting with the rotating blades. Thus, the significant unsteadiness detected by the calculation models used is due only to the presence of the volute tongue in the flow. According to [8], URANS calculations cannot adequately provide the surface pressure fluctuations needed for broadband noise prediction. Thus, the spectrum component, other than the fundamental harmonic peak could be numerical.

8. **Conclusions**

3D unsteady flow in a centrifugal fan has been studied in this paper using URANS equations. The overall behavior of the fan has been validated experimentally at different flow rates.

The analysis of the flow morphology showed the influence of the geometry design on the aerodynamic performance of the fan.

The analysis of the pressure fluctuations around the lateral surface of the volute and the force fluctuations indicated that the main source of perturbation and unsteadiness in a squirrel cage fan is the volute tongue zone.

The spectral analysis of the sound pressure level computed by the FW-H equation showed that the main source of tonal noise in the fan investigated is the aerodynamic interaction between the impeller and the volute tongue.

It should be interesting to extend this work by:

- Validating the fluctuating pressures computed on the lateral surface of the volute casing.
- Validating the acoustic spectra using measurements in an echoic room.
- Using Large Eddy Simulation (LES) approach to feed acoustic models.

REFERENCES

1. Gabi, M. and Klemm, T.: Numerical and experimental investigations of cross-flow fans, *Journal of Computational and Applied Mechanics*, **5**, (2004), 251-261.
2. Sandra, V.S. and Santolarya, C.: Experimental study on the aeroacoustic behaviour of a forward-curved blades centrifugal fan. *ASME Journal of Fluid Engineering*, **277**, (1999), 276-281.
3. Thakur, S., Lin, W. and Wright, J.: Prediction of flow in centrifugal blower using quasi-steady rotor-stator models. *Journal of Engineering Mechanics*, (2002), 1039-1049.
4. Cho, Y. and Moon, Y.J.: Discrete noise prediction of variable pitch cross-flow fans by unsteady Navier-Stokes computations. *ASME Journal of Fluids Engineering*, **125**, (2003), 543-550.
5. Kim, K.Y. and Seo, S.J.: Shape Optimization of forward-curved-blade centrifugal fan with Navier-Stokes analysis. *ASME Journal of Fluids Engineering*, **126**, (2004), 735-742.
6. ISO 5801.: Industrial fans - Performance testing using standardized airways, (1997).

7. Williams, F. and Hawkings, J.E.: Sound generation by turbulence and surfaces in arbitrary motion. *Phi. Trans. Roy. Soc.*, A264, (1969).

8. Brentner, K.S., and Farassat, F.: An analytical comparison of the acoustic analogy and Kirchhoff formulation for moving surfaces. *AIAA Journal*, **36**(8), (1998).